

# Segmentation of vessels using weighted local variances and an active contour model

W. K. Law and Albert C. S. Chung

Lo Kwee-Seong Medical Image Analysis Laboratory, Department of Computer Science,  
The Hong Kong University of Science and Technology, Clear Water Bay, Hong Kong  
{maxlawwk, achung}@cs.ust.hk

## Abstract

*Performing segmentation of vasculature with blurry and low contrast boundaries in noisy images is a challenging problem. This paper presents a novel approach to segmenting blood vessels using weighted local variances and an active contour model. In this work, the vessel boundary orientation is estimated locally based on the orientation that minimizes the weighted local variance. Such estimation is less sensitive to noise compared with other common approaches. The edge clearness is measured by the ratio of weighted local variances obtained along different orientations. It is independent of the edge intensity contrast and capable of locating weak boundaries. Integrating the orientation and clearness of edges, an active contour model is employed to align contours that match the contour tangent direction and edge orientation. The proposed method is validated by two synthetic images and two real cases. It is experimentally shown that our method is suitable for dealing with noisy images which consist of structures having blurry and low contrast boundaries, such as blood vessels.*

## 1. Introduction

Active contour models have been used widely for segmentation of medical images, e.g. vessel segmentation in angiograms. To partition vascular structures, it is common to use image gradient as a criterion to locate vessel boundaries. For instance, Lorigo *et al.* [7] presented a gradient magnitude based vessel segmentation technique which utilizes the level set framework [9] to represent and evolve contours. The evolution of the moving contours is governed by a speed term that is inversely proportional to the image gradient magnitude. As such, the contours eventually halt over the object boundaries. Xu and Prince proposed the Gradient Vector Flow [13] which models gradient magnitude as the source of attractive forces for drawing contours to the object boundaries having high gradient magni-

tude. However, for some noisy images, e.g. digital subtraction angiography (DSA) and retinal angiography, the vessel boundaries are blurry and with low contrast. These factors can lead to low gradient magnitude on the object boundaries and affect adversely the segmentation accuracy of the gradient magnitude based active contour approaches.

To deal with low contrast object boundaries in noisy images, Chan and Vese [2] demonstrated that the task of segmentation can be achieved by solving the minimal partition problem. Instead of using gradient information, this approach separates target objects from the image background by minimizing the global sum variance calculated from the regions that are inside and outside contours. Nevertheless, due to the inhomogeneous intensity values of vessels and image background, the resultant contours can enclose both the dark vessel portions and bright background regions as the same region. In addition, the regularization term based on total contour length for noise elimination tends to annihilate elongated contours.

Without using region statistics and length regularization term, Vasilevskiy and Siddiqi introduced the Flux Maximizing Geometric Flows [11] which incorporate both the gradient magnitude and direction information to detect weak edges. By maximizing the inward (or outward) flux, the contour evolution is guided by the edge orientation and finally stopped on the zero-crossing boundaries of the discrete approximated Laplacian operation. The major advantage is that it is sensitive to weak edges and robust to noisy structures. Along the same research line, Xiang *et al.* proposed an elastic interaction model [12] which also employs information of both edge orientation and magnitude. This method is highly sensitive to low contrast boundaries. As it will be shown later in the experiments, the intensity variation inside vascular structures generates significant intensity gradient along the long and narrow vessels. This undesired discontinuity can halt the contour evolution at these regions. On the other hand, the Gaussian operation smooths the vessel boundaries and, at the same time, can cause contour leakage though the noisy region attached to vessel bound-

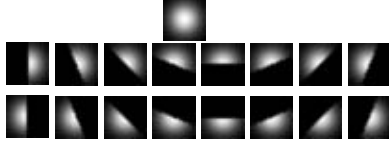


Figure 1. *Top:*  $G_{\sigma=4}$ . *Middle:*  $g_{1,\theta}(x, y)$ . *Bottom:*  $g_{2,\theta}(x, y)$ .

aries.

In this paper, we propose to use the weighted local variances and an active contour model for vessel segmentation. Edge orientation in an image is defined by the orientation that minimizes the weighted local variance. The corresponding edge clearness is calculated using the ratio of variances obtained along different orientations. Based on the estimated edge information, including edge orientation and clearness, a new energy functional is formulated to draw contours to minimize the angular difference between the contours and object boundaries. The major advantage of this work is that the proposed method is less sensitive to intensity fluctuation by noise and intensity variation along vessels, and is able to locate weak and low contrast boundaries. The weighted local variance based edge orientation estimation is compared with two edge orientation estimators using synthetic images. Our method is tested on two real images including a DSA image and a retinal angiogram. It is experimentally shown that the weighted local variance based edge information and active contour approach is suitable for dealing with elongated vasculature with blurry and low contrast boundaries in noisy images.

## 2. Methodology

### 2.1. Weighted Local Variance

To extract edge information based on weighted local variance (WLV), including edge orientation and clearness, we first consider the Heaviside function,

$$H_{\theta}(x, y) = \begin{cases} 0 & \text{i f } t_{\theta}(x, y) \leq -\epsilon, \\ \frac{1}{2}(\sin \frac{\pi t_{\theta}(x, y)}{2\epsilon} + 1) & \text{i f } |t_{\theta}(x, y)| < \epsilon, \\ 1 & \text{i f } t_{\theta}(x, y) \geq \epsilon, \end{cases} \quad (1)$$

where  $t_{\theta}(x, y) = x \cos \theta + y \sin \theta$ , orientation  $\theta$  represents the gradient direction of the Heaviside function, and  $\epsilon$  is a small constant. This function creates a straight line oriented along  $\theta_{\perp}$ , where  $\theta_{\perp} = \theta + \frac{\pi}{2}$ , for smoothly separating a region into two half planes, one has values of '1' and the other plane has values of '0'. At each pixel  $(x, y)$ , WLV is calculated within a small, local region using two half sided Gaussian kernels,

$$\begin{aligned} g_{1,\theta}(x, y) &= G_{\sigma}(x, y) \cdot H_{\theta}(x, y), \\ g_{2,\theta}(x, y) &= G_{\sigma}(x, y) \cdot (1 - H_{\theta}(x, y)), \end{aligned} \quad (2)$$

where  $G_{\sigma}$  is a Gaussian kernel with detection scale equals to  $\sigma$ . It shows that each half plane, as defined and separated

by the Heaviside function (Equation 1), is multiplied with a Gaussian kernel. The scale parameter of the Gaussian kernel,  $\sigma$ , determines the size of objects to be detected. In our application, segmentation of vasculature, the value of  $\sigma$  should be defined roughly smaller than the widths of vessels. Examples of  $g_{1,\theta}$  and  $g_{2,\theta}$  with  $\epsilon = 0.1$ ,  $\sigma = 4$ , and different orientations  $\theta$  are illustrated in Figure 1. Using the half sided Gaussian kernels in Equation 2, given an arbitrary orientation  $\theta$ , WLV at pixel  $(x, y)$  is defined as

$$\begin{aligned} \text{Var}_{\theta}(x, y) &= \int \{g'_{1,\theta}(u, v) \cdot \\ & (I(x + u, y + v) - \mu_{1,\theta}(x, y))^2 + g'_{2,\theta}(u, v) \cdot \\ & (I(x + u, y + v) - \mu_{2,\theta}(x, y))^2\} dudv, \end{aligned} \quad (3)$$

where  $I(x, y)$  represents the intensity at  $(x, y)$ ,  $g'_{1,\theta}$  and  $g'_{2,\theta}$  are the normalized versions of  $g_{1,\theta}$  and  $g_{2,\theta}$  respectively,

$$g'_{i,\theta}(x, y) = \frac{g_{i,\theta}(x, y)}{\int g_{i,\theta}(u, v) dudv}, i = \{1, 2\}, \quad (4)$$

and  $\mu_{1,\theta}(x, y)$  and  $\mu_{2,\theta}(x, y)$  are the weighted intensity averages of their corresponding half planes separated by a straight line along orientation  $\theta_{\perp}$ ,

$$\mu_{i,\theta}(x, y) = \int g'_{i,\theta}(u, v) \cdot I(x + u, y + v) dudv, i = \{1, 2\}. \quad (5)$$

The weighted local variance (WLV),  $\text{Var}_{\theta}(x, y)$  (Equation 3), can be viewed as a weighted sum of squared differences between the intensity of the neighboring pixels around  $(x, y)$  and its corresponding weighted intensity average,  $\mu_{1,\theta}$  or  $\mu_{2,\theta}$ . A small value of WLV along a particular orientation  $\theta$  implies that pixels are well partitioned into two groups by a straight line along the orientation  $\theta_{\perp}$ . WLV at each pixel changes as  $\theta$  varies and attains minimum when the orientation of the straight line aligned with the object boundaries. Therefore, we formulate the relation between WLV and the edge orientation  $\omega(x, y)$  at  $(x, y)$  as,

$$\begin{aligned} \omega(x, y) &= \arg \min_{\theta \in [0, \pi)} \{\text{Var}_{\theta}(x, y)\} + \frac{\pi}{2} \\ &= \arg \min_{\theta \in [0, \pi)} \left\{ \int \{g'_{1,\theta}(u, v) \cdot \right. \\ & (I(x + u, y + v) - \mu_{1,\theta}(x, y))^2 + g'_{2,\theta}(u, v) \cdot \\ & \left. (I(x + u, y + v) - \mu_{2,\theta}(x, y))^2\} dudv \right\} + \frac{\pi}{2}. \end{aligned} \quad (6)$$

As we shall see in Section 3, estimation of edge orientation using WLV is less sensitive to noise. Our method is different from other conventional operators such as first derivative of Gaussian, Laplacian operators or quadrature filters [3, 4, 6]. When estimating the edge orientation, since

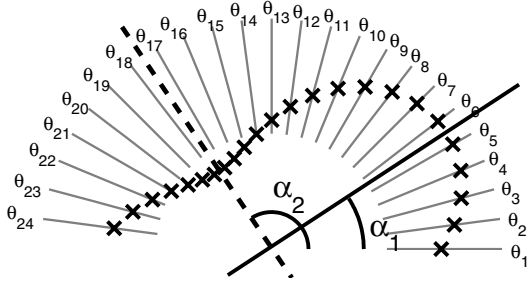


Figure 2. An example of polar space for a pixel.  $K = 24$ , the  $\alpha$  is found according to  $V_1, V_2, \dots, V_{24}$ . The numbers and the gray lines represent the orientation of  $\theta_k$ . The black crosses are the points  $(\sqrt{\text{Var}_{\theta_k}}, \theta_k)$ , where  $k \in \{1, 2, \dots, 24\}$ . The solid line and the dotted line are the straight lines  $(r, \alpha_1)$ ,  $(r, \alpha_2)$  respectively.

noisy pixels can boost the values of WLW along all orientations, there is little impact on finding the orientation by minimizing WLW. It is because pixels are weighted isotropically in the calculation of WLW. Thus, the noisy pixels affect the values of WLW by roughly the same amount disregard to the kernel orientation. This situation holds unless noisy pixels form a group and create an edge which has higher contrast than the object boundary.

The edge orientation  $\omega(x, y)$  can be estimated using the relation stated in Equation 6. However, this equation cannot be solved analytically. In this paper, we propose to discretize  $\theta$  as  $\theta_k = \frac{k\pi}{K}$ ,  $k \in \{1, 2, \dots, K\}$  and estimate  $\omega(x, y)$  in a continuous fashion. A very accurate estimation requires  $\theta$  being discretized in a high angular resolution. However, probing the WLW in a high angular resolution for a discrete estimation is computationally expensive. Without using a high angular resolution, we set  $K = 24$  in this work.

To estimate the continuous edge orientation  $\omega(x, y)$  at a pixel, we first employ polar space to observe the relationship between WLWs obtained along all discrete orientations. The WLWs are represented as points using the polar coordinates  $(\sqrt{\text{Var}_{\theta_k}}, \theta_k)$  in polar space (See Figure 2). When the orientations  $\theta_k$  are close to the perpendicular direction of the edge (i.e.  $\theta_k + \frac{\pi}{2}$  is the edge orientation), the values of WLW become smaller than those parallel to the edge. As shown in Figure 2, the points along these orientations are packed closely to the origin and sparsely along the other orientations. To capture this relation, we use the sum squared perpendicular distances from the points  $(\sqrt{\text{Var}_{\theta_k}}, \theta_k)$  to a straight line passing through the origin along an orientation  $\alpha$ . The distance is defined as,

$$D_{(x,y)}(\alpha) = \sum_{k=1}^K \text{Var}_{\theta_k}(x, y) \cos^2(\theta_k - \alpha). \quad (7)$$

Therefore, the edge orientation can be computed using the

above equation which approximates the Equation 6,

$$\begin{aligned} \omega(x, y) &= \arg \max_{\alpha \in [0, \pi)} \{D_{(x,y)}(\alpha)\}, \\ &= \arg \max_{\alpha \in [0, \pi)} \sum_{k=1}^K \text{Var}_{\theta_k}(x, y) \cos^2(\theta_k - \alpha) \end{aligned} \quad (8)$$

The solution of Equation 8 is obtained by computing the zero occurrence of the first derivative of  $D$  with respect to the orientation  $\alpha$ ,

$$\tan 2\alpha = \frac{\sum_{k=1}^K \text{Var}_{\theta_k}(x, y) \cdot \sin 2\theta_k}{\sum_{k=1}^K \text{Var}_{\theta_k}(x, y) \cdot \cos 2\theta_k}, \alpha \in [0, \pi). \quad (9)$$

Solving the above equation, two solutions  $\alpha_1$  and  $\alpha_2$  can be found analytically for each pixel. The angles  $\alpha_1$  and  $\alpha_2$  are orthogonal to each other. They represent the edge and gradient orientation respectively. An graphical example of solving  $\alpha$  is given in Figure 2. In this example, in terms of the perpendicular distance, the points are packed closer to the line along the orientation  $\alpha_1$ . It implies that the variances along the orientation  $\alpha_2$  are smaller, hence,  $\alpha_2$  is the gradient orientation and  $\alpha_1$  is the edge orientation in this example.

Apart from the edge orientation estimation, WLWs along different orientations also reflect the confidence about the estimated orientation. For instance, the difference between the WLW values along the edge orientation and gradient orientation should be large for a sharp straight edge. In contrast, such difference should be small for a noisy edge. Therefore, it is natural to measure the edge clearness using the sum squared perpendicular distances along edge and gradient orientations. We therefore define a ratio,

$$M(x, y) = \frac{|D_{(x,y)}(\alpha_1) - D_{(x,y)}(\alpha_2)|}{D_{(x,y)}(\alpha_1) + D_{(x,y)}(\alpha_2) + \rho}, \quad (10)$$

where  $\rho$  is a small constant to prevent singularity in homogeneous regions that WLWs are zero along all orientations. The Equation 10 measures the ratio between the difference and sum of the sum squared perpendicular distances along edge and gradient orientations. As the WLW values vary largely in different orientations for sharp and clear edges, the ratio  $M$  (Equation 10) can give a large value. On the other hand, a pixel with small value of ratio  $M$  belongs to noise or an unclear edge.

An important property is that the ratio  $M$  does not depend on the intensity contrast. It can be illustrated by considering two arbitrary image patches  $S$  and  $R$  which have different intensity contrast and brightness but are related by  $R = c \cdot S + b$ . The terms  $c$  and  $b$  are constants representing the differences in intensity contrast and brightness respectively. Hence, it can be shown that  $\text{Var}_{\theta}^R(x, y) = c^2 \cdot \text{Var}_{\theta}^S(x, y)$  and  $D_{(x,y)}^R(\alpha) = c^2 \cdot D_{(x,y)}^S(\alpha)$ . The constant term  $c$  is finally canceled in Equation 10, for calculation of the clearness of edges. Distinct from other common

edge detectors or operators such as Sobel, Roberts, Prewitt, Laplacian operators and quadrature filters [3, 4], the clearness of edge of WLW does not depend on intensity contrast. This is particularly essential to deal with the vascular images that consist of both low contrast vessels and noisy vessels.

## 2.2. Active Contour Model

In the previous section, we derive a WLW approach to estimating edge orientation and clearness of edges. We now formulate an active contour model which employs the estimated edge orientation and clearness for performing segmentation on vascular images. Let  $C(l) = [x(l) \ y(l)]^T$  be a closed curve parameterized by the length parameter  $l$ , where  $0 \leq l \leq L$ . The tangent direction of this curve is denoted as  $\gamma(l)$ , where  $-\pi \leq \gamma(l) < \pi, \forall l$ . As such, the optimal contours should minimize the angular discrepancies between  $\omega(C(l))$  and  $\gamma(C(l))$  along the curve. However, the edge direction is ambiguous along two directions,  $\omega(C(l))$  and  $\omega(C(l)) - \pi$ . Such ambiguity can be eliminated by comparing the average intensity of the local regions in two different sides of the edge. The edge direction is defined as  $\omega(x, y) + \pi \cdot (\frac{S(x, y)}{2} - 0.5)$ , where  $S(x, y) = \text{sign}(\mu_{1, \omega(x, y)}(x, y) - \mu_{2, \omega(x, y)}(x, y))$ .

The desired resultant curve is designed to align in the same direction as the object boundaries, which maximizes the following functional,

$$\begin{aligned} F(C) &= \oint_C \cos\{\gamma(C(l)) - (\omega(C(l)) \\ &\quad + \pi(\frac{S(x, y)}{2} - 0.5))\} dl, \\ &= \oint_C S(C(l)) \cdot \{\cos(\gamma(C(l))) \cos(\omega(C(l))) \\ &\quad + \sin(\gamma(C(l))) \sin(\omega(C(l)))\} dl. \end{aligned} \quad (11)$$

We make this functional favor clear edges by giving large weights for those boundaries having high value in Equation 10, and substitute  $\cos(\gamma(C(l))) = \frac{\partial}{\partial l} x(l)$  and  $\sin(\gamma(C(l))) = \frac{\partial}{\partial l} y(l)$ ,

$$\begin{aligned} F_M(C) &= \oint_C S(C(l)) \cdot M(C(l)) \cdot \\ &\quad \{\cos(\omega(C(l))) \frac{\partial}{\partial l} x(l) \\ &\quad + \sin(\omega(C(l))) \frac{\partial}{\partial l} y(l)\} dl. \end{aligned} \quad (12)$$

Applying the Green's theorem, we have,

$$\begin{aligned} F_M(C) &= \int_{\text{Inside}(C)} \left\{ \frac{\partial}{\partial x} (S(x, y) M(x, y) \sin(\omega(x, y))) \right. \\ &\quad \left. - \frac{\partial}{\partial y} (S(x, y) M(x, y) \cos(\omega(x, y))) \right\} dx dy. \end{aligned} \quad (13)$$

Using the zero level of a level set surface [9] to represent moving contours, the motion of the level set surface is  $\phi_t = E|\nabla\phi|$ , where  $E$  is the scalar value of the curve evolution speed in its normal direction. Solving  $E = \frac{\delta F_M(C)}{\delta C}$ , we have,

$$\begin{aligned} E(x, y) &= \left\{ \frac{\partial}{\partial x} (S(x, y) M(x, y) \sin(\omega(x, y))) \right. \\ &\quad \left. - \frac{\partial}{\partial y} (S(x, y) M(x, y) \cos(\omega(x, y))) \right\} \end{aligned} \quad (14)$$

As a result, the term  $E$  represents the rate of change of the edge information including the change of the orientation and clearness. It has large value inside objects and near the clear and straight boundaries. Therefore, the initial contour can be chosen by thresholding a proportion of regions that has the highest  $E$  values. In practice, we smooth the term  $E$  slightly before performing thresholding, and smooth the resultant contours obtained from thresholding using a curvature flow to ensure the initial seeds are located only in the major vessels but not noisy regions.

## 2.3. Implementation

In our implementation, WLW is computed along 24 discrete orientations and  $K = 24$  for Equation 7 and Equation 9. It requires calculation of WLVs 24 times at each pixel. To speed up the calculation, the integration in Equation 3 is reformulated in the form of convolution, which can be computed in the Fourier domain efficiently,

$$\begin{aligned} &\text{Var}_\theta(x, y) \\ &= \int \{g'_{1, \theta}(u, v) \cdot (I(x + u, y + v) - \mu_{1, \theta}(x, y))^2 \\ &\quad + g'_{2, \theta}(u, v) \cdot (I(x + u, y + v) - \mu_{2, \theta}(x, y))^2\} \\ &\quad dudv, \\ &\text{since } g'_1 \text{ and } g'_2 \text{ are sum-to-one,} \\ &= \int \{g'_{1, \theta}(u, v) \cdot I^2(x + u, y + v) - \mu_{1, \theta}^2(x, y) \\ &\quad + g'_{2, \theta}(u, v) \cdot I^2(x + u, y + v) - \mu_{2, \theta}^2(x, y)\} \\ &\quad dudv, \\ &\text{flipping } g'_1 \text{ and } g'_2 \text{ and writing as convolution,} \\ &= \{g'_{1, \theta}(x, y) + g'_{2, \theta}(x, y)\} * I^2(x, y) \quad (15) \\ &\quad - \{g'_{1, \theta}(x, y) * I(x, y)\}^2 - \{g'_{2, \theta}(x, y) * I(x, y)\}^2. \end{aligned}$$

Therefore, the integration in Equation 3 is formulated as convolution and calculated as multiplication in the Fourier domain. The running time of calculating WLVs along  $K$  different orientations is reduced from  $O(KN^2)$  to  $O(KN \log N)$  for an image having  $N$  pixels.

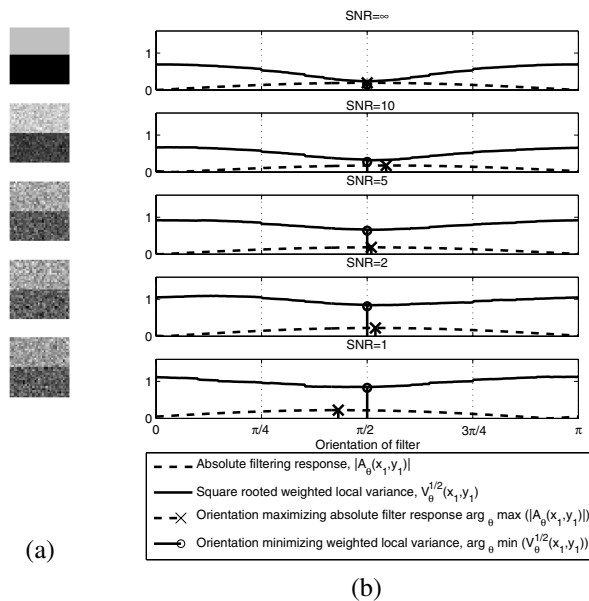


Figure 3. (a) From top to bottom, a clear horizontal edge and the image is corrupted using Gaussian noise with SNR=  $\infty$ , 10, 5, 2, 1. (b) Plots of WLVs and filtering responses of the first derivatives of Gaussian along different orientations. The orientation estimation results are marked as circles and crosses for WLW and the first derivatives of Gaussian respectively.

### 3. Experiments

In this section, we study the accuracy in orientation estimation by weighted local variance (WLV) and show the segmentation results obtained by the active contour model using WLV. Two synthetic images are utilized to illustrate the robustness of WLV-based orientation estimation against noise. Besides, using two real angiograms, the proposed active contour model has been compared with three other active contour approaches.

#### 3.1. Edge orientation estimation

The first experiment used a horizontal edge, as shown in Figure 3a. By adding different levels of Gaussian noise (no noise, SNR=10, 5, 2 and 1) on this image, we measured the values of  $\sqrt{\text{Var}_\theta}$  at the center pixel  $(x_1, y_1)$  along 512 discrete orientations,  $\theta$ , ranging from 0 to  $\pi$  (Figure 3b). The angles that minimize  $\sqrt{\text{Var}_\theta}$  in different noise levels are marked in the figure. The result is compared with the

	WLV	The first derivatives of Gaussian
No noise	0	0
SNR=10	$4.90 \times 10^{-5}$	0.045001
SNR=5	0.000413	0.081156
SNR=2	0.025881	0.119140
SNR=1	0.056744	0.123655

Table 1. Average absolute acute angular differences (in radians) between the estimated orientation and the orientation of the horizontal edge.

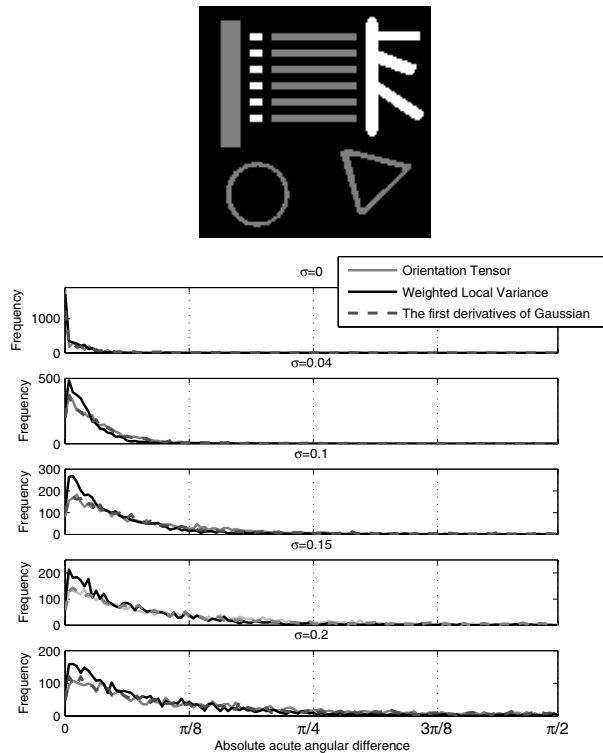


Figure 4. Top: A  $128 \times 128$  synthetic image. Bottom: The angular discrepancies between the estimated orientation and the reference orientation. Zero angular difference at the left side of the x-axis represents a correct estimation (no discrepancy),  $\pi/2$  means the estimated orientation is perpendicular to the reference orientation. "Frequency" in the y-axis represents the number of occurrences of a particular orientation discrepancy. High number of occurrences in low discrepancy implies better performance.

first derivatives of Gaussian, which are commonly used for detecting intensity discontinuities [1, 8]. Considering the relation between the filtering responses,  $I * G_y = (I * G)_y$  and  $I * G_x = (I * G)_x$ , the orientation estimation by the first derivatives of Gaussian can be viewed as the orientation of the gradient vector obtained from a smoothed image. Hence, such information is also widely utilized in different active contour models, such as [11, 12]. The first derivatives of Gaussian along x-direction and y-direction are given by,

$$G_x = -\frac{x}{2\pi\sigma^4} e^{-\frac{x^2+y^2}{2\sigma^2}} \quad \text{and} \quad G_y = -\frac{y}{2\pi\sigma^4} e^{-\frac{x^2+y^2}{2\sigma^2}},$$

respectively. We convolved the image with these two filters and their responses are denoted as  $A_0(x_1, y_1)$  and  $A_{\pi/2}(x_1, y_1)$ . The filtering responses in other orientations  $\theta$  were synthesized by  $A_\theta = A_0 \cos \theta + A_{\pi/2} \sin \theta$ . The edge orientation for maximizing the absolute filtering response magnitude was computed using  $\arctan \frac{I * G_y}{I * G_x}$  in the quadrant of  $[0, \pi)$ .

The scale of the Gaussian functions for both methods was set to be 2. In Figure 3b, we can see how noise affects the edge orientation estimation by WLW and the first derivatives of Gaussian. The estimated orientations according to

$A_\theta$  are inaccurate in the noisy images. In contrast, although the values of  $\text{Var}_\theta$  are increased in the noisy images, the estimation using WLV is more accurate. As mentioned in the previous section, noisy pixels can boost the values of WLV along all orientations. But it has little impact on the accuracy in estimating the orientation that minimizes  $\text{Var}_\theta$ . To further investigate the performance of WLV, the same experiment was iterated 1000 times. The absolute acute angular discrepancies  $|\theta_{\text{estimated}} - \theta_{\text{truth}}|$  were measured each time for both methods. Its average values are listed in Table 1. WLV yields lower discrepancies in all noisy cases. It shows that the orientation estimation by WLV is more accurate than those by the first derivatives of Gaussian.

The performance of WLV was now examined using a more complicated synthetic image (Figure 4). This image contains tubular structures with different widths and intensity values (0.2 for the gray regions and 1 for the white regions). It also consists of curved boundaries, junctions and corners. In this experiment, WLV was compared with the first derivatives of Gaussian and "Orientation Tensor" [6] (OT). For OT-based method, the edge orientation is estimated by performing eigen decomposition on an orientation tensor, which is calculated from the filter responses of three complex valued quadrature filters. The bandwidth and center frequency were set to be 2 and  $\pi/2\sqrt{2}$  according to [4]. The scale parameter of the Gaussian function used by WLV and the first derivatives of Gaussian was 2.

The edge orientation estimation by the three methods were measured at the positions of the object boundaries. Comparison was performed on the images which were corrupted by a Gaussian noise with different values of standard deviation  $\sigma$ . The histograms of  $|\theta_{\text{reference}} - \theta_{\text{estimated}}|$  for different noisy images are shown in Figure 4.  $\theta_{\text{reference}}$  was obtained according to the intensity gradient on the smoothed version of the synthetic image in the quadrant of  $[0, \pi)$  (by a Gaussian filter, scale parameter equals to 1). For the image without noise,  $\sigma = 0$  in Figure 4, all methods show only small discrepancies which were caused by the differences in handling corners and junctions. Comparing the results between the noisy images and the image without noise, more occurrences of large discrepancies are observed for noisy images. It is found that the orientation estimation by WLV is more accurate than the other two methods as WLV has generally lower discrepancies.

### 3.2. Real Image Segmentation

The proposed active contour model using WLV is applied on the real images. A DSA image (Figure 5a) obtained from the Department of Diagnostic Radiology and Organ Imaging, Prince of Wales Hospital, Hong Kong, and a retinal angiogram (Figure 7a) provided by the "DRIVE database" [10] were selected for the experiments. In the images, four intensity profiles for different lines of interest

are plotted to illustrate intensity variations in vessels and background for understanding the behaviors of different approaches. Two comparisons were performed between the proposed method and three different approaches including (1) "Active Contours without Edges" (ACWE) [2], (2) "A New Active Contour Method based on Elastic Interaction" (ACEI) [12] and (3) "Flux Maximizing Geometric Flows" (FM) [11].

Figure 5 shows a DSA image which consists of a vertical vessel with limited background noise. The intensity inside the vessel is dropped significantly in several positions (see Figures 5b-f for lines of interest and their corresponding intensity profiles). Consistently, all approaches have no leakage because of the low level of background noise. However, ACWE (Figure 6a) only selects the brightest segment of the vessel because of the large intensity variations in the vessel. For ACEI, the resultant contour (Figure 6b) halts at two positions (Figures 5c and 5f). For FM, several positions inside the vessel was recognized as vessel boundaries (Figure 6c). The disconnected contours cannot be merged to enclose the entire vessel. In contrast, WLV does not prefer relatively weak edges across the vessel. Therefore, the proposed method can handle intensity variations inside the vessel, and the contour can propagate through the dim regions to capture the whole vessel (Figure 6d).

The second experiment includes a retinal angiogram, as shown in Figure 7a. The background intensity increases, as shown along the line of interest (Figure 7c). Figure 7f shows an intensity drop inside a small vessel branch. The results of ACWE are shown in Figure 8a. ACWE selects the bright background region in the right side of the image as vessel region. Several dim vessel portions are excluded. For ACEI, the contour initialization, as mentioned in [12], mixes up the vessel and background regions in the right part of the image. Thus, two initial contours were placed manually inside the vessels. Leakage occurred in several positions (Figure 8b), especially in the right portion of the image, where the boundary contrast is small (see Figures 5b, 5d and 5e for lines of interest and their corresponding intensity profiles). For FM, since there is no leakage (Figure 8c), the performance of FM is better than that of ACEI and ACWE. But, its contour halts at the position marked by line  $f$  in Figure 7b (see Figure 7f for its intensity profile). For the proposed method, neither leakage nor undesired discontinuity is found and both vessels are successfully captured (Figure 8d).

## 4. Conclusion and Discussion

In this paper, we have presented the use of the weighted local variance (WLV) for extracting edge information, including edge orientation and clearness, to perform the active contour based vessel segmentation. The edge orientation using WLV is demonstrated to be robust to noise in

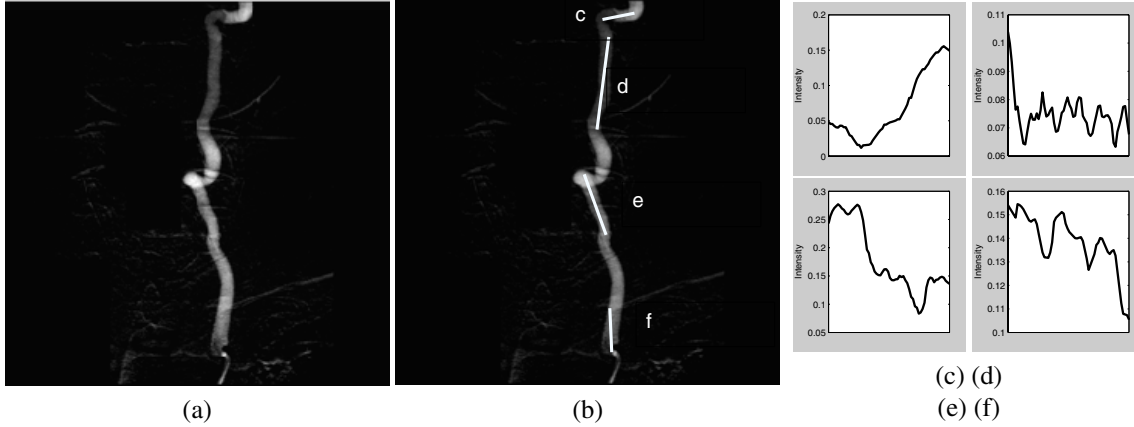


Figure 5. (a) A  $256 \times 256$  DSA image. (b) Showing the lines of interest where intensity profiles are plotted in (c-f). (c) The intensity profile is plotted along line *c* in (b) from left to right. (d-f) The intensity profiles are plotted along the corresponding lines in (b) from top to bottom.

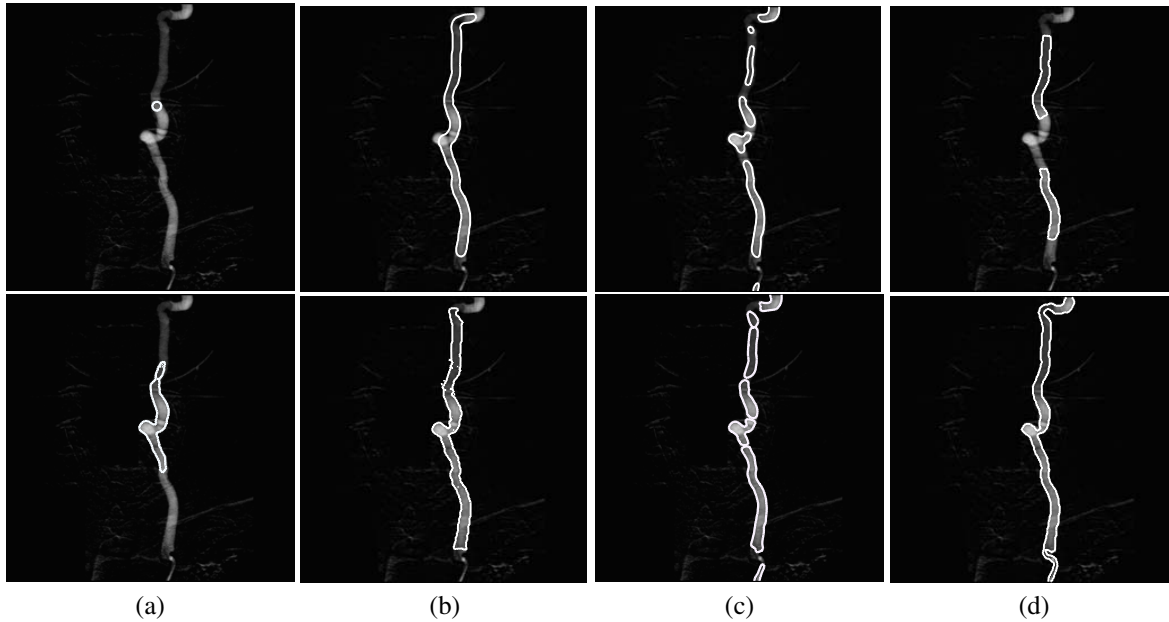


Figure 6. Top row: Initial contours. Bottom row: Final results. (a) ACWE, manually selected initial contour,  $\mu = 0.001 \cdot 255^2$ ,  $\lambda_1 = \lambda_2 = 1$ ,  $\nu = 0$ ,  $h = 1$ . (b) ACEL, initial contour obtained automatically as in [12],  $\sigma_1 = 2$ ,  $\sigma_2 = 10$ ,  $\mu = 0.0015$ . (c) FM,  $r = \{1, 2, 3, 4\}$ , image pre-processed with  $G_{\sigma=2}$  initial contour obtained automatically from regions with highest 5% inward flux which is further smoothed under curvature flow for 500 steps. (d) The proposed method,  $\sigma = 2$ ,  $\rho = 0.0001$ ,  $\epsilon = 0.1$ , initial contour obtained automatically from smoothing the term  $E$  using  $G_{\sigma=1}$  and choosing the regions with highest 5% value of  $E$  which is further smoothed under curvature flow for 500 steps.

the two synthetic image experiments. Using the estimated edge information, the active contour based segmentation has been validated using two real angiograms and compared with three related approaches. It shows that our method is suitable for handling vasculature having blurry and low contrast boundaries in noisy images.

If we consider a vector field,  $[u \ v]^T$ , which integrates both the edge orientation and clearness of WLW,  $[u \ v]^T = S \cdot M[\cos(\omega + \frac{\pi}{2}) \ \sin(\omega + \frac{\pi}{2})]^T$ , where  $\omega + \frac{\pi}{2}$  is the gradient direction, the energy functional in Equation 13 becomes  $\int_{Inside(C)} (\frac{\partial u}{\partial x} + \frac{\partial v}{\partial y}) dx dy$ . It yields an interesting relation to the work in [5] on edge integration based on the Laplacian

operation, where the vector field  $[u \ v]^T$  mentioned above can be utilized to substitute the vector field of the image gradient. Subsequently, it is possible to formulate the WLW-based edge information as a vector field and be incorporated in other works which employ image gradient, such as [5, 11, 12].

## References

- [1] J. Canny. A computational approach to edge detection. In *IEEE. PAMI.*, volume 8, pages 679–698, 1986. 5
- [2] T. Chan and L. Vese. Active contour without edges. In *IEEE. TIP.*, volume 10, pages 266–277, 2001. 1, 6

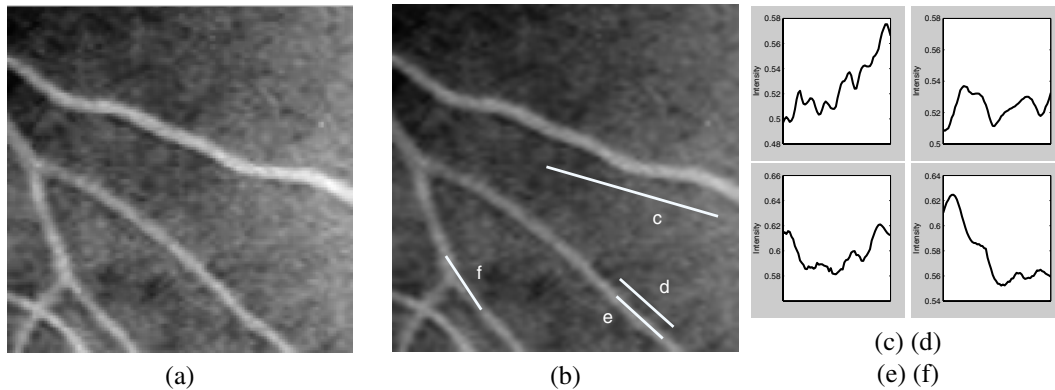


Figure 7. (a) A  $128 \times 128$  retinal angiogram. (b) Showing the lines of interest where intensity profiles are plotted in (c-f). (c-f) The intensity profiles are plotted along the corresponding lines in (b) from left to right.

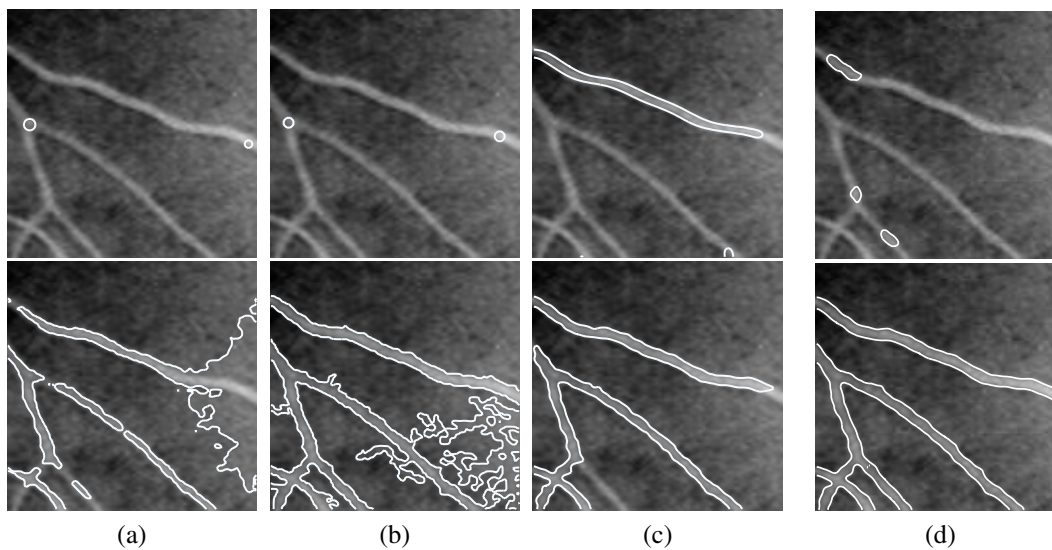


Figure 8. Top row: Initial contours. Bottom row: Final results. (a) ACWE, manually selected initial contour,  $\mu = 0.004 \cdot 255^2$ ,  $\lambda_1 = \lambda_2 = 1$ ,  $\nu = 0$ ,  $h = 1$ . (b) ACEI, manually selected initial contour,  $\sigma_1 = 1.5$ ,  $\mu = 0.0015$ . (c) FM,  $r = \{2, 3, 4\}$ , image pre-processed with  $G_{\sigma=1}$  initial contour obtained automatically from regions with highest 5% inward flux which is further smoothed under curvature flow for 2000 steps. (d) The proposed method,  $\sigma = 1.5$ ,  $\rho = 0.0001$ ,  $\epsilon = 0.1$ , initial contour obtained automatically from smoothing the term  $E$  and choosing the regions with highest 5% value of  $E$  which is further smoothed under curvature flow for 500 steps.

- [3] T. Folsom and R. Pinter. Primitive features by steering, quadrateure, and scale. In *IEEE. PAMI.*, volume 20, pages 1161–1173, 1998. 2, 4
- [4] G. Granlund and H. Knutsson. *Signal processing for computer vision*. Kluwer Academic Publishers, 1995. 2, 4, 6
- [5] R. Kimmel and A. Bruckstein. Regularized laplacian zero crossings as optimal edge integrators. In *IJCV.*, volume 53 of 3, pages 225–243, 2003. 7
- [6] H. Knutsson. Representing local structure using tensors. In *The 6th Scandinavian Conf. on Image Anal.*, pages 244–251, 1989. 2, 6
- [7] L. Lorigo, O. Faugeras, and et al. CURVES: curve evolution for vessel segmentation. *Medical Image Analysis*, 5(3):195–206, 2001. 1
- [8] W. Ma and B. Manjunath. Edgeflow: A technique for boundary detection and image segmentation. In *IEEE. TIP.*, volume 9, pages 1375–1388, 2000. 5
- [9] S. Osher and J. Sethian. Fronts propagating with curvature dependent speed: algorithms based on hamilton-jacobi formulations. In *J. on Comp. Phys.*, volume 79, pages 12–49, 1988. 1, 4
- [10] J. Staal, M. Abramoff, M. Niemeijer, M. Viergever, and B. Ginneken. Ridge based vessel segmentation in color images of the retina. In *IEEE. TMI.*, volume 23, pages 501–509, 2004. 6
- [11] A. Vasilevskiy and K. Siddiqi. Flux maximizing geometric flows. In *IEEE. Trans. PAMI.*, volume 24, pages 1565–1578, 2002. 1, 5, 6, 7
- [12] Y. Xiang, A. Chung, and J. Ye. A new active contour method based on elastic interaction. In *IEEE. CVPR.*, volume 1, pages 452–457, 2005. 1, 5, 6, 7
- [13] C. Xu and J. Prince. Snakes, shapes, and gradient vector flow. In *IEEE. TIP.*, volume 7, pages 359–369, 1998. 1